14th European Signal Processing Conference (EUSIPCO 2006), Florence, Italy, September 4-8, 2006, copyright by EURASIP

MODELLING AND MANIPULATION OF POLARIMETRIC ANTENNA BEAM PATTERNS VIA SPHERICAL HARMONICS

Giovanni Del Galdo[1], *Jörg Lotze*[1], *Markus Landmann*[2], *and Martin Haardt*[1]

Ilmenau University of Technology, Ilmenau, Germany
[1] Communications Research Laboratory - [2] Measurements Engineering Laboratory
{giovanni.delgaldo, markus.landmann, martin.haardt}@tu-ilmenau.de
http://www.tu-ilmenau.de/crl

ABSTRACT

Measured antenna responses, namely their beam patterns with respect to the vertical and horizontal polarizations, play a major role in realistic wireless channel modelling as well as in parameter estimation techniques. The representations commonly used suffer from drawbacks introduced by the spherical coordinate system which is affected by two knots at the poles. In general, all methods which describe the beam pattern with a matrix fail in correctly reproducing its inherent spherical symmetry. In this contribution we propose the use of the Spherical Fourier Transformation (SFT) which allows the description of the beam pattern via spherical harmonics. This mathematical tool, well known in other fields of science, is rather new to wireless communications. In this context, the main applications of the SFT include the efficient description of a beam pattern, noise filtering, the precise interpolation in the spherical Fourier domain, and the possibility to obtain an equivalent description of the beam pattern for an arbitrary coordinate system. The latter allows us to improve an existing 2-D FFT based technique: the Effective Aperture Distribution Function (EADF).

1. INTRODUCTION

Considering the radiation pattern of the sensors of an antenna array is crucial to any parameter estimation technique [1] and undoubtedly an important aspect of channel modelling as well [2]. The far-field radiation pattern of an array sensor is usually described with its field strength for the so-called vertical and horizontal polarizations [3]. In fact, the vector $\boldsymbol{E}(\theta,\varphi,r)$, which represents the electric field at distance r for a specific elevation θ and azimuth φ, is transversal to the direction of propagation and therefore can be described as

$$\boldsymbol{E}(\theta,\phi,r) = \sqrt{\eta}\ \frac{\mathrm{e}^{-j\,\gamma\,r}}{r}\left[f_\theta(\theta,\phi)\,\boldsymbol{u}_\theta + f_\phi(\theta,\phi)\,\boldsymbol{u}_\phi\right], \qquad (1)$$

where γ is the propagation constant, and η is the intrinsic impedance of the medium. The vectors with unit norm $\boldsymbol{u}_\theta$ and $\boldsymbol{u}_\phi$ are directed towards θ and φ. The complex functions f_θ and f_ϕ express the antenna directivity functions (in voltage) for the two polarizations, vertical and horizontal, respectively. Their phases represent the relative phase shift which leads to linear, circular or elliptical polarizations.

Traditionally the beam pattern for each polarization is stored in form of a matrix obtained by sampling the pattern on a regular grid on the sphere, namely a grid obtained by uniformly sampling azimuth and elevation. This is a straightforward representation which is used to measure (calibrate) an antenna array [2]. For each point in azimuth and elevation the response of each sensor to the vertical and the horizontal excitation is measured. With this approach the coupling between the array sensors is included.

At this point the information can be treated as a traditional 2-dimensional discrete signal so that spectral analysis tools can be used. This principle sets the basis for the Effective Aperture Distribution Function (EADF) proposed in [2], which implements a 2-D FFT applied on the periodified beam pattern. In the spectral domain it is possible to store the information more efficiently, to perform noise filtering (in case of a measured beam pattern) as well as to carry out interpolation in the transformed domain.

Unfortunately, the transformation from the spherical coordinate system to a 2-dimensional representation is strongly non-linear. In the new representation, the samples are treated as if they were uniformly spaced from one another, which in the original coordinate system is evidently not true. Furthermore, the particular periodicity existing in the spherical system is lost. The EADF partly solves the periodicity issue by considering an elevation angle which is defined for a 360° range. By doing this, the beam pattern description is periodic along elevation as well, at the expense of introducing redundancy. Nonetheless, the strong non-linearity of the transformation is impossible to overcome. Note that this drawback is marginal when the gain of the antenna in the direction of the poles of the coordinate system chosen is negligible. However, when dealing with antenna arrays which employ sensors pointing in all directions, such as the spherical array used in [4] or the Omni-Directional patch Array (ODA) in [5], we cannot disregard this problem.

One solution is to use different coordinate systems for different sensors, with respect to the direction of the main lobe. To do so we can either measure certain sensors on a different grid, or interpolate the available data to obtain a representation in another coordinate system. The first solution is not feasible from a practical point of view. The interpolation, either in angle domain or in the 2-D Fourier domain (as proposed in [2]) is also impractical due to the high errors introduced around the poles by the non-linearity of the 2-D description.

In this contribution we propose a solution to these problems by exploiting the natural Fourier domain for spherical functions, which is obtained via the Spherical Fourier Transform (SFT). The use of the SFT leads to interesting interpretations and several applications valuable for channel modelling and parameter estimation techniques.

Section 2 introduces the SFT for the description and manipulation of beam patterns. Section 3 describes its applications, while Section 4 proposes an SFT based improvement of the EADF. Finally, Section 5 presents the conclusions.

2. THE SPHERICAL FOURIER TRANSFORM

Following the representation given in equation (1) it is apparent that both f_θ and f_φ are not continuous functions on the sphere, because their value changes at the north and south poles for different azimuths. To overcome this problem we derive an equivalent description by expressing the pattern in terms of unit basis vectors $\boldsymbol{u}_x$, $\boldsymbol{u}_y$, and $\boldsymbol{u}_z$ pointing to the x, y, and z axes. Equation (1) becomes

$$\boldsymbol{E}(\theta,\phi,r) = \sqrt{\eta}\ \frac{\mathrm{e}^{-j\,\gamma\,r}}{r}\left[f_x\boldsymbol{u}_x + f_y\boldsymbol{u}_y + f_z\boldsymbol{u}_z\right], \qquad (2)$$

where the directivities f_x, f_y, and f_z are functions of θ and φ, and are continuous on the sphere. The transformation functions are

$$f_x \quad = \quad -f_\theta \cdot \sin(\theta) \cdot \cos(\varphi) - f_\varphi \cdot \sin(\varphi)$$

$$\begin{aligned} f_y &= -f_\theta \cdot \sin(\theta) \cdot \sin(\varphi) + f_\varphi \cdot \cos(\varphi) \\ f_z &= f_\theta \cdot \cos(\theta), \end{aligned} \tag{3}$$

where we omit the angle dependency (θ, ϕ) for simplicity.

In order to use spectral methods for spherical problems one possibility is to use the Spherical Wave Expansion (SWE) as in [6, 7]. The SWE is based on the vector spherical wavefunctions, which are a simplification of the tensor spherical harmonics [8]. However, this approach has the disadvantage that the Fourier coefficients are cumbersome to compute numerically, although theoretically straightforward. For instance, in [6], the coefficients of the expansion are estimated solving a least squares problem, whereas in [7] they are obtained by methods of numerical matching.

We propose to use the scalar Spherical Fourier Transform (SFT) [8] applied separately on f_x, f_y, and f_z. The SFT is the equivalent of the 1-dimensional Fourier series, although its basis functions are defined on the sphere. These functions are usually referred to as *Spherical Harmonics* (SH). The spherical harmonics represent the *kernel* of the SFT, analogous to the complex expontentials for the 1-D Fourier series. The spherical harmonics can be defined on any coordinate system and are continuous functions on the sphere, thus dependent on two parameters only. For convenience we use the spherical coordinate system. Let $\theta \in \left[-\frac{\pi}{2}, \frac{\pi}{2}\right]$ and $\varphi \in [-\pi, \pi]$ be elevation and azimuth, respectively. The north pole corresponds to elevation $\theta = \frac{\pi}{2}$. The spherical harmonic $Y_l^m(\theta, \varphi)$ of order m and level l is defined as:

$$Y_l^m(\theta, \varphi) = P_l^{|m|}(\sin(-\theta)) \cdot \mathrm{e}^{jm\varphi}, \tag{4}$$

where the $P_l^m(\cdot)$ is the *associated Legendre function* and is derived from the *Legendre polynomial* $P_l(x)$:

$$\begin{aligned} P_l^m(x) &= \left((2l+1)\frac{(l-m)!}{(l+m)!}\right)^{\frac{1}{2}} \left(1-x^2\right) \frac{\mathrm{d}^m}{\mathrm{d}x^m} P_l(x) \\ P_l(x) &= \frac{1}{2^l l!} \frac{\mathrm{d}^l}{\mathrm{d}x^l} \left(x^2-1\right)^l. \end{aligned}$$

The level l can only assume positive integer values and plays the equivalent role of the frequency in the 1-dimensional Fourier series. In fact, $l = 0$ corresponds to the DC component, while higher levels correspond to basis functions increasingly more varying. For the l-th level there are $2 \cdot l + 1$ modes. In other words, $m \in [-l, l]$. We define, for convenience, the index set $\mathscr{I}$ as

$$\mathscr{I} = \{(l, m) : l \in \mathbb{N}_0,\ m \in \mathbb{Z},\ -l \le m \le l\}. \tag{5}$$

The functions defined in equation (4) represent the basis functions of the spherical Fourier transform. They form a complete orthogonal system in the Hilbert space $\mathsf{L}^2\left(\mathbb{S}^2\right)$, i.e., the space of all square integrable functions on the 2-sphere $\mathbb{S}^2$ [9]. Two functions f and g are orthogonal on the sphere when their inner product $< f, g >$ is equal to zero, where

$$< f, g >= \frac{1}{4\pi} \int_{-\pi}^{\pi} \int_{-\frac{\pi}{2}}^{\frac{\pi}{2}} f(\theta, \varphi)\ g^\star(\theta, \varphi)\ \sin(\theta)\ \mathrm{d}\theta \mathrm{d}\varphi, \tag{6}$$

where $(\cdot)^\star$ denotes the conjugate operator. Hence, the orthogonality of the basis functions can be mathematically expressed as follows:

$$< Y_l^m, Y_n^k >= \delta_{n,l}\delta_{m,k}, \text{ for } (m, l) \text{ and } (k, n) \in \mathscr{I}, \tag{7}$$

where $\delta_{m,k}$ is the Kronecker delta, so that $\delta_{m,k} = 1$ for $m = k$ and zero otherwise.

The spherical Fourier transform and its inverse are defined as follows:

$$a_l^m(f) = < f, Y_l^m > \tag{8}$$

$$f = \sum_{(l,m)\in\mathscr{I}} a_l^m(f) \cdot Y_l^m, \tag{9}$$

where $a_l^m(f)$ is the spherical Fourier coefficient for the l-th level and m-th mode. From equations (8) and (9) the analogy with the 1-dimensional Fourier Series appears evident.

2.1 The discrete spherical fourier transform

Similarly to the 1-D case, we call a function $f(\theta, \varphi)$ on the $\mathbb{S}^2$ sphere a *band-limited function* when it can be completely described by a limited number L of spherical Fourier frequencies, so that $l = [0,\ 1,\ \ldots, L-1]$. The total number of Fourier coefficients M is then $M = L^2$. It is possible to compute these coefficients without error, and thus solve the integral associated with equation (8), from a finite number S of samples on the sphere. This problem is known as *quadrature* or *cubature* [10]. The value of S depends obviously on L and on the sampling grid chosen. There exist many quadrature rules tailored for spherical harmonics. We present the two most common:

- **Gauss-Legendre quadrature**
  This grid consists of a Gauss quadrature in the elevation and a uniform one in the azimuthal direction. Let $\mathscr{G}_{\mathrm{GL}}$ define the grid points on the sphere as follows

$$\mathscr{G}_{\mathrm{GL}} = \begin{cases} (\theta_h, \varphi_k) = \left(\cos^{-1}(z_h) - \frac{\pi}{2}, \frac{k\pi}{N}\right), \text{ where} \\ h = [0,\ 1,\ \ldots,\ N],\ \ k = [0,\ 1,\ \ldots,\ 2N-1], \end{cases} \tag{10}$$

  where z_j are the zeros of the Legendre polynomial of order $(N+1)$. Note that the azimuth is uniformly sampled with a separation angle of $\frac{\pi}{N}$. The total number of samples on the sphere is $S_{\mathrm{GL}} = (N+1) \times 2N$. The coefficients are computed as:

$$a_l^m(f) = \sum_{h=0}^{N-1} \left(\frac{1}{2N} \sum_{k=-N}^{N-1} f(\theta_h, \varphi_k)\, \mathrm{e}^{-jm\varphi_k} \right) \cdot \cdot P_l^m(\sin(-\theta_h)) \cdot \cos(\theta_h) \cdot w_{h,\mathrm{GL}}^N, \tag{11}$$

  where $(\theta_h, \varphi_k) \in \mathscr{G}_{\mathrm{GL}}$ and $w_{h,\mathrm{GL}}^N$ are Gaussian weights along the longitudes.
- **Chebyshev knots – uniform quadrature**
  This quadrature considers a uniform grid for both elevation and azimuth. Let $\mathscr{G}_{\mathrm{Ch}}$ define the grid points on the sphere as follows

$$\mathscr{G}_{\mathrm{Ch}} = \begin{cases} (\theta_h, \varphi_k) = \left(\frac{h\pi}{2N}, \frac{k\pi}{N}\right), \quad \text{where} \\ h = [0,\ 1,\ \ldots,\ 2N],\ \ k = [0,\ \ldots,\ 2N-1]. \end{cases} \tag{12}$$

  The Chebyshev knots are obtained by uniformly sampling both elevation (with sampling interval $\Delta\theta = \frac{\pi}{2N}$) and azimuth (with $\Delta\varphi = \frac{\pi}{N}$). The total number of samples on the sphere is $S_{\mathrm{Ch}} = (2N+1) \times 2N$. The coefficients are computed as:

$$a_l^m(f) = \sum_{h=0}^{2N} \varepsilon_h^{(2N)} \left(\frac{1}{2N} \sum_{k=-N}^{N-1} f(\theta_h, \varphi_k)\, \mathrm{e}^{-jm\varphi_k} \right) \cdot \cdot P_l^m(\sin(-\theta_h)) \cdot w_{h,\mathrm{Ch}}^N, \tag{13}$$

  where $(\theta_h, \varphi_k) \in \mathscr{G}_{\mathrm{Ch}}$,

$$\varepsilon_h^{(N)} = \begin{cases} \frac{1}{2} & \text{for } h = 0,\ N \\ 1 & \text{for } h = 1,\ 2,\ \ldots,\ N-1 \end{cases} \tag{14}$$

  and $w_{h,\mathrm{Ch}}^N$ are the weights computed as

$$w_{h,\mathrm{Ch}}^N = \frac{1}{2N} \sum_{s=0}^{N} \varepsilon_h^{(N)} \frac{2}{1-4s^2} \cos\left(\frac{hs\pi}{N}\right). \tag{15}$$

The following expression, similarly to the sampling theorem, sets the minimum value for the parameter N appearing in equations (10) and (12), with respect to the highest level L contained in the function on the sphere to be studied:

$$N \ge \frac{3L+1}{2}. \tag{16}$$

M	L	N	S_{GL}	S_{Ch}
100	10	16	17×32	33×32
441	21	32	33×64	65×64
1764	42	64	65×128	129×128
7225	85	128	129×256	257×256

Table 1: Relation between number of Fourier coefficients M and points on the sphere S for the Gauss-Legendre and Chebyshev quadratures. The term S is expressed as number of samples along elevation times the number of samples along azimuth.

Note that equation (16) does not guarantee that a function defined on a certain grid with parameter N can be described by $L \leq \frac{2N-1}{3}+1$ levels. The equation simply states that with a given N we can determine for how many levels L we can compute the Fourier coefficients exactly. However, even for twice the number of levels defined by equation (16) we commit very small errors, on the order of -50 dB. Table 1 shows the total number of complex coefficients M in the frequency domain, the corresponding minimum value for the parameter N, and the number of samples needed on the sphere S_{GL} and S_{Ch} following a Gauss-Legendre and a Chebishev quadrature, respectively. The Gauss-Legendre grid does not comprise samples at the poles, and is almost uniformly distributed along elevation. The Legendre polynomials can be correctly integrated with much fewer points for the Gauss-Legendre quadrature, so that, as seen in Table 1, approximately half the points are needed in comparison to the Chebyshev grid.

2.2 The rotation operator

It is possible to rotate freely a function $g(\theta,\varphi)$ by applying the so called *Wigner D-function* to the spherical Fourier coefficients [8]. According to Euler's rotation theorem [11], an arbitrary rotation can be accomplished by three basic rotations characterized by three angles, known as *Euler angles*, α, β, and δ about three known axes. There are several conventions for Euler angles, depending on the axes about which the rotations are carried out. The convention best fit for SH consists in applying a rotation of α about the z axis, followed by a rotation of β about the new y axis, and finally rotating of δ about the new z axis. Let $\tilde{g}(\theta,\varphi)$ be the transformed version of $g(\theta,\varphi)$, derived by a rotation of (α,β,δ) as described above. Thanks to the Wigner-Eckart theorem [8] we can write

$$\begin{aligned} g(\theta,\varphi) &= \sum_{(l,m)\in\mathscr{I}} a_l^m(g)\cdot Y_l^m \\ \tilde{g}(\theta,\varphi) &= \sum_{(l,m)\in\mathscr{I}} \tilde{a}_l^m(g)\cdot Y_l^m \\ \tilde{a}_l^m(g) &= \sum_{m'=-l}^{l} D^l_{mm'}(\alpha,\beta,\delta)\, a_l^{m'}(g), \end{aligned} \tag{17}$$

where the Wigner-D function $D^l_{mm'}$ is defined as

$$D^l_{mm'}(\alpha,\beta,\delta) = \mathrm{e}^{-jm\alpha}\cdot d^l_{mm'}(\beta)\cdot \mathrm{e}^{-jm'\delta}, \tag{18}$$

and

$$d^l_{mm'} = (-1)^{l+m}\ \sqrt{(l+m)!\,(l-m)!\,(l+m')!\,(l-m')!}\ \cdot \\ \cdot \sum_{k\in\mathscr{K}} (-1)^k \frac{\cos^{2k-m-m'}\left(\frac{\beta}{2}\right)\sin^{2l+m+m'-2k}\left(\frac{\beta}{2}\right)}{k!\,(l+m-k)!\,(l+m'-k)!\,(k-m-m')!}.$$

The summation is carried out for the index $k\in\mathscr{K}$ so that:

$$\mathscr{K} = \left\{ \begin{array}{l} m\in\mathbb{N}_0, \quad \text{and} \\ \max[0,-(m-m')] \leq m \leq \min[l-m, l+m']. \end{array} \right. \tag{19}$$

When we apply the rotation operator we rotate the complex directivity functions f_x, f_y, and f_z on the sphere. When doing so we implicitly rotate the basis vectors $\boldsymbol{u}_x$, $\boldsymbol{u}_y$, and $\boldsymbol{u}_z$ as well. Let $\tilde{f}_{x'}$, $\tilde{f}_{y'}$, and $\tilde{f}_{z'}$ be the rotated functions obtained by applying equation (17) onto f_x, f_y, and f_z. The subscripts x', y', and z' describe the rotated axes. The desired rotated directivity functions $\tilde{f}_x$, $\tilde{f}_y$, and $\tilde{f}_z$ expressed in terms of $\boldsymbol{u}_x$, $\boldsymbol{u}_y$, and $\boldsymbol{u}_z$ can be computed as follows

$$\begin{bmatrix} \tilde{f}_x \\ \tilde{f}_y \\ \tilde{f}_z \end{bmatrix} = \boldsymbol{R}_z(\alpha)\cdot\boldsymbol{R}_y(\beta)\cdot\boldsymbol{R}_z(\delta)\cdot \begin{bmatrix} \tilde{f}_{x'} \\ \tilde{f}_{y'} \\ \tilde{f}_{z'} \end{bmatrix}, \tag{20}$$

where the rotation matrices $\boldsymbol{R}_z(\cdot)$ and $\boldsymbol{R}_y(\cdot)$ are

$$\boldsymbol{R}_z(\cdot) = \begin{bmatrix} \cos(\cdot) & \sin(\cdot) & 0 \\ -\sin(\cdot) & \cos(\cdot) & 0 \\ 0 & 0 & 1 \end{bmatrix}, \quad \boldsymbol{R}_y(\cdot) = \begin{bmatrix} \cos(\cdot) & 0 & -\sin(\cdot) \\ 0 & 1 & 0 \\ \sin(\cdot) & 0 & \cos(\cdot) \end{bmatrix}.$$

An example is given in Section 3.3.

2.3 Power spectrum and white noise

For a set of spherical Fourier coefficients $a_l^m(f)$ obtained from a SFT on the function $f(\theta,\varphi)$ we define the *power spectrum* $\Phi(l)$as

$$\Phi(l) = \Sigma_{m=-l}^{l}\ |a_l^m(f)|^2, \tag{21}$$

and the *cumulative power function* $\Gamma(l)$ as

$$\Gamma(l) = \Sigma_{k=0}^{l-1}\Phi(l), \tag{22}$$

so that $\Gamma(l)$ describes the amount of power present in the levels $0,\ 1,\ \ldots l-1$. Assuming that the function $f(\theta,\varphi)$ can be described by L levels, we define the power $P_L(f)$ to be

$$P_L(f) = <f,f> = \Sigma_{l=0}^{L-1}\Phi(l) = \Gamma(L). \tag{23}$$

Equation (23) represents the Parseval theorem for the spherical Fourier domain.

We model the measurement noise as band-limited white Gaussian noise in the angle domain. This process, $w(\theta,\varphi)$, can be described with spherical harmonics as follows

$$w(\theta,\varphi) = \Sigma_{l=0}^{L_w-1}\ \Sigma_{m=-l}^{l}\ w_l^m, \tag{24}$$

where the coefficients w_l^m have both real and imaginary parts $\sim\ \mathscr{N}(0,\frac{\sigma_w^2}{2})$, and L_w is the *bandwidth* of the noise, delimiting the number of levels needed to describe it. Its power spectrum is $\Phi(l) = (2l+1)\cdot\sigma_w^2$ and the total noise power is $L_w^2\cdot\sigma_w^2$. Interestingly, white noise in the spherical harmonics domain has the same power spectral density for all modes but a power spectrum $\Phi(l)$ which grows linearly, as the number of modes increases linearly with the level l.

3. THE APPLICATIONS OF THE SFT

3.1 Compressing, noise filtering, and SNR estimation

As Table 1 shows, the spherical Fourier coefficients are a more compact way to describe a function on the sphere than storing the values of the function sampled on the traditional uniform grid in angle domain. Furthermore, similarly to the EADF (i.e., a 2-D DFT), the SFT applied on an oversampled beam pattern obtains a compression of the information in the Fourier domain, so that even a smaller number of samples is needed to fully describe the pattern. At the same time we are able to perform noise filtering and to estimate the Signal to Noise Ratio (SNR). Let $f_\theta(\theta,\varphi)^{\mathrm{meas}}$ and $f_\varphi(\theta,\varphi)^{\mathrm{meas}}$ be the measured directivities of an antenna (or array sensor) as described in (1). When calibrating an antenna with a known dual-polarized probe antenna we cannot prevent an unknown constant phase difference ψ affecting the data so that

$$f_\theta(\theta,\varphi)^{\mathrm{meas}} = f_\theta(\theta,\varphi) \tag{25}$$

$$f_\varphi(\theta,\varphi)^{\mathrm{meas}} = f_\varphi(\theta,\varphi)\cdot\mathrm{e}^{j\psi}, \tag{26}$$

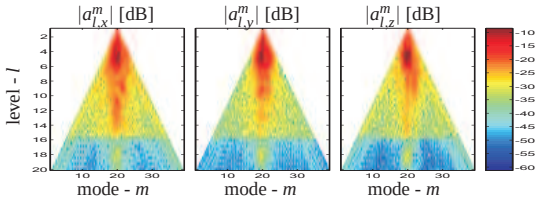

Figure 1: Spherical Fourier coefficients for the measured beam pattern of one element of an Omni-Directional patch Array (ODA)[1].

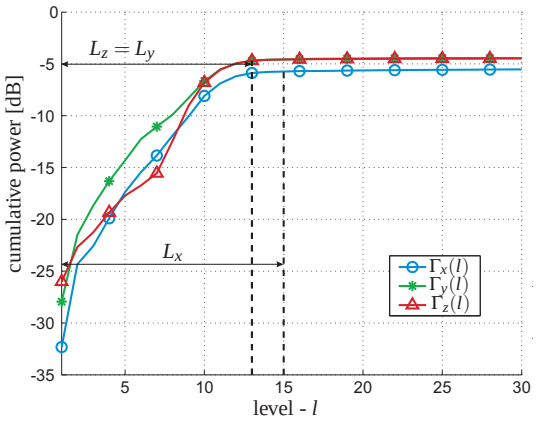

Figure 2: Cumulative power functions for the beam pattern expressed in x, y and z. The bandwidths L_x, L_y, and L_z indicate the levels for which $\Gamma(l)$ reaches 96 % of the total power.

where $f_\theta(\theta,\varphi)$ and $f_\varphi(\theta,\varphi)$ are the directivity functions unaffected by the phase shift. The phase shift ψ introduces discontinuities at the poles in the beam patterns f_x and f_y. To overcome this problem we use the corrected directivity function $f_\varphi(\theta,\varphi)^{\text{corr}}$ obtained by $f_\varphi(\theta,\varphi)^{\text{corr}} = f_\varphi(\theta,\varphi)^{\text{meas}} \cdot \mathrm{e}^{-j\hat{\psi}}$, where $\hat{\psi}$ is the estimated phase shift chosen such that the values of the beam patterns in y and z are constant for all azimuths at the poles, i.e., for $\theta = \pm\frac{\pi}{2}$. We perform the transformation expressed in equation (3) on $f_\theta(\theta,\varphi)^{\text{meas}}$ and $f_\varphi(\theta,\varphi)^{\text{corr}}$ to obtain the functions f_x, f_y, and f_z. Then, we carry out three separate discrete SFT's on f_x, f_y, and f_z to obtain the spherical Fourier coefficients $a^m_{l,x}$, $a^m_{l,y}$, and $a^m_{l,z}$, respectively, up to L levels. Figure 1 shows the coefficients for one of the 25 elements of an Omni-Directional patch Array (ODA)[1] which was measured in an anechoic chamber with a 2° sampling interval in both elevation and azimuth. Figure 2 shows the corresponding cumulative power functions computed as in equation (22). For this antenna we have approximately 35 % of the power directed towards y and z, and the remaining 30 % towards x. Let L_x, L_y, and L_z be the bandwidths of the beam pattern expressed in x, y, and z, defined as the levels at which the cumulative power functions reach 96 % of the total power. The remaining levels (between L_x, L_y, and L_z and the levels at which the functions reach the total power) are affected by noise only, and are therefore valuable for estimating the power of the noise. Under the assumption of additive Gaussian noise we estimate the power σ_w^2 possessed by each Fourier coefficient by averaging $|a_l^m|^2$ for all the modes and levels within the range just described. Let $P_{L_x}(f_x)$, $P_{L_y}(f_y)$, and $P_{L_z}(f_z)$ be the powers of the beam patterns for the corresponding bandwidths L_x, L_y, and L_z. Then, we estimate the Signal to Noise Ratio (SNR) ρ_x for f_x as

$$\rho_x = \frac{P_{L_x}(f_x) - \sigma_w^2 \cdot L_x^2}{\sigma_w^2 \cdot L_x^2}, \tag{27}$$

[1]We thank Elektrobit Testing Ltd. for providing the antenna calibration data [5]

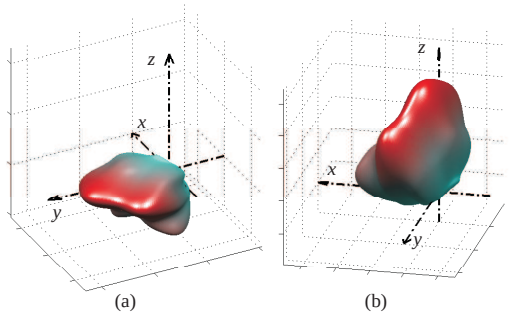

Figure 3: Power directivity $b(\theta,\varphi)$ for the same beam pattern for two different orientations: (a) as it was measured, (b) rotated with $\alpha = 30°$, $\beta = 90°$, and $\delta = 90°$.

where ρ_y and ρ_z are computed in the same way. The SNR of the whole beam pattern ρ is simply the average. For the measured beam pattern we obtained an average SNR of approximately 25 dB.

3.2 Interpolation in the spherical Fourier domain

Once the spherical Fourier description of the beam pattern has been computed it is possible to carry out Fourier interpolation. To obtain the values of the functions f_x, f_y, and f_z in an arbitrary direction (θ_0,φ_0) we can simply apply the inverse SFT as in equation (9). Unfortunately we cannot count on an algorithm such as the FFT, since along latitudes we need to perform a Legendre transform. Recently [12, 13] fast approximate and exact transforms have been proposed. Their computational complexity is however difficult to assess and up to now only complexity orders have been computed. For instance, the exact transform requires $\mathcal{O}(N^2\log^2 N)$. However, considering the small number of levels L needed for our applications (around 20), these results do not apply.

3.3 Rotation and rotation invariant descriptors

Let us now consider another measured beam pattern whose power directivity function $b(\theta,\varphi) = |f_\theta|^2 + |f_\varphi|^2$ can be seen in plot (a) of Figure 3. The beam pattern belongs to one of 24 elements of a Stacked Polarimetric Uniform Circular Patch Array (SPUCPA) which was measured at Ilmenau University of Technology on a uniform 3° sampling grid. Plot (b) shows the very same beam pattern rotated by $\alpha = 30°$, $\beta = 90°$, and $\delta = 90°$, as described in Section 2.2, so that the main lobe points directly towards the north pole. Figure 4 shows the cumulative power functions for f_x, f_y, and f_z for the beam pattern in the two orientations just described. Note that for the two orientations we have different functions f_x, f_y, and f_z and therefore different power spectra and cumulative power functions. The *total cumulative power function* $\Gamma_{\text{tot}}(l)$ is computed as

$$\Gamma_{\text{tot}}(l) = \Sigma_{k=0}^{l-1}\Phi_{\text{tot}}(l), \tag{28}$$

where the *total power spectrum* $\Phi_{\text{tot}}(l)$ defined as

$$\Phi_{\text{tot}}(l) = \Phi_x(l) + \Phi_y(l) + \Phi_z(l), \tag{29}$$

is a rotation invariant descriptor of the beam pattern. In other words, with different orientations of the beam pattern we will have different spherical Fourier coefficients. However, the total power $\Phi_{\text{tot}}(l)$ for each level l is fixed and is not dependent on the orientation or coordinate system chosen. This property can be derived by the rotation invariance of tensor spherical harmonics as they are irreducible tensor products of scalar spherical harmonics [8].

In [2] the EADF was used to define the bandwidth of a beam pattern, as the size of the limited support in frequency domain needed to describe it. However, this description depends on the coordinate system chosen and is therefore not related to the physical properties of the beam pattern. On the other hand, the functions

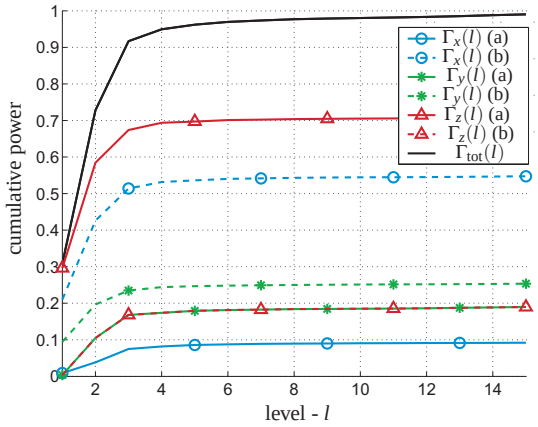

Figure 4: Cumulative power functions expressed in x, y and z for the measured beam pattern (a), and for its rotated version (b) (see Figure 3). The total cumulative power function $\Gamma_{\text{tot}}(l)$ is a rotation invariant descriptor of the beam pattern.

$\Phi_{\text{tot}}(l)$ and $\Gamma_{\text{tot}}(l)$ are rotation invariant and are therefore ideal to define a bandwidth L_b for the beam pattern.

We can do so by setting L_b equal to the maximum level needed to represent a certain percentage of the power. Furthermore, by comparing L_b to the paramter L from equation (16) we can determine whether our sampling grid was dense enough.

4. IMPROVING THE EADF

The efficiency of the Effective Aperture Distribution Function in compressing the information depends on the beam pattern itself and the spherical coordinate system chosen to represent it [2]. In fact, the beam pattern rotated as in plot (a) of Figure 3 will be much more compressed by the EADF than rotated as in plot (b). In addition, when interpolating in the 2-D Fourier domain, the EADF commits higher errors around the poles. Consequently, the beam pattern (b) will suffer from a higher interpolation error as the one in (a) because a significant amount of power is directed towards the north pole. For many array geometries this problem can be avoided by selecting a proper coordinate system, so that all beam patterns have little power in the direction of the poles. However, in the case of sphere-like geometries such as the one used in [4] or the Omni-Directional patch Array (ODA) in [5], one or more sensors will be directed towards a pole and this issue cannot be disregarded. The spherical harmonics offer an elegant solution to this problem. However the fast algorithms to compute the SFT are still much slower compared to the FFT implemented by the EADF. We propose to improve the EADF by measuring the array sensors with an arbitrary coordinate system and compute the spherical Fourier coefficients as explained in Section 3.1. For those sensors pointing towards the poles we can still employ the EADF but in another coordinate system. The description of the beam pattern in a more convenient coordinate system can be obtained by rotating the beam pattern in the spherical Fourier domain, as explained in Section 2.2. Thereby, we neither lose information nor add any interpolation noise. The transformation between two spherical coordinate systems are quite inexpensive and add very little computational complexity to the already very efficient EADF.

5. CONCLUSIONS

In this contribution we propose the use of the scalar Spherical Fourier Transformation (SFT) which allows the description of polarimetric beam patterns via spherical harmonics. This mathematical tool, well known in other fields of science, is rather new to wireless communications. The main applications of the SFT include the efficient description of a beam pattern, noise filtering, the precise interpolation in the spherical Fourier domain, and the possibility to obtain an equivalent description of the beam pattern for an arbitrary coordinate system. The latter allows us to improve an existing 2-D FFT based technique: the Effective Aperture Distribution Function (EADF). The SFT leads to a rotation invariant descriptor which allows us to define a bandwidth for any given beam pattern as the number of spherical frequencies (levels) needed to describe it. This tool is valuable for assessing whether the sampling grid in angle domain is dense enough. Quadrature rules suggest more efficient ways of measuring the beam patterns optimizing the sampling grid and thus minimizing measurement time.

Acknowledgements

The authors gratefully acknowledge the partial support of the EC funded network of excellence NEWCOM, and of the German Research Foundation (Deutsche Forschungsgemeinschaft, DFG) under contract no. HA 2239/1-1

REFERENCES

[1] H. Krim and M. Viberg, "Two decades of array signal processing research: The parametric approach," *IEEE Signal Processing Magazine*, vol. 13, no. 4, pp. 67–94, Jul 1996.

[2] M. Landmann and G. Del Galdo, "Efficient antenna description for MIMO channel modelling and estimation," *European Microwave Week, Amsterdam, The Netherlands*, 2004.

[3] S. Drabowitch, *Modern Antennas*, Chapman & Hall, London, 1998.

[4] K. Kalliola, H. Laitinen, L.I. Vaskelainen, and P. Vainikainen, "Real-time 3-d spatial-temporal dual-polarized measurement of wideband radio channel at mobile station," *IEEE Transactions on Instrumentation and Measurement*, vol. 49, no. 2, pp. 439–448, 2000.

[5] J. Hamalainen, R. Wichman, J.-P. Nuutinen, J. Ylitalo, and T. Jamsa, "Analysis and measurements for indoor polarization MIMO in 5.25 ghz band," in *Proc. IEEE Vehicular Technology Conference, VTC Spring*, June 2005, vol. 1, pp. 252–256.

[6] P. Koivisto, "Reduction of errors in antenna radiation patterns using optimally truncated spherical wave expansion," *Progress in Electromagnetics Research, PIER 47*, pp. 313–333, 2004.

[7] O. Klemp, G. Armbrecht, and H. Eul, "Analytical modeling of polarization diversity performance for frequency-independent planar multiarm antennas," *in Proc. WSA Workshop on Smart Antennas, Castle Reisensburg near Ulm, Germany*, Mar. 2006.

[8] D. A. Varshalovich, A.N. Moskalev, and V. K. Kherosonskii, Eds., *Quantum Theory of Angular Momentum*, World Scientific, Singapore, 1998.

[9] G. Sansone, *Elementary Notions of Hilbert Space*, Dover, New York, 1991.

[10] F. Sprengel, "Can we use the known fast spherical fourier transform in numerical meteorology," *GMD Report 142*, 2001, downloadable from `http://www.bi.fraunhofer.de/publications/report/0142/`.

[11] E. W. Weisstein, Ed., *Euler Angles*, From MathWorld–A Wolfram Web Resource, 2006, `http://mathworld.wolfram.com/EulerAngles.html`.

[12] D. Potts, G. Steidl, and M. Tasche, "Fast and stable algorithms for discrete spherical Fourier transforms," *Linear Algebra and Applications, 275*, pp. 433–450, 1998.

[13] M. J. Mohlenkamp, "A fast transform for spherical harmonics," *Journal of Fourier Analysis and Applications, 5*, pp. 159–184, 1999.